Supplementary data

Enhanced single and simultaneous As(III) adsorption in Pearl River Delta water by hexylamine functionalized vermiculite

Zubair Ahmed[a,f], Pingxiao Wu[a, b, c, d, e, *],

Yijing Xu[a], Hareef Ahmed Keerio[g], Jiayan Wu[a], Quanyun Ye[a], Wenchao Niu[a], Meiqing Chen[a], Zhi Dang[a.]

[a] School of Environment and Energy, South China University of Technology, Guangzhou 510006, P.R. China.

[b] The Key Lab of Pollution Control and Ecosystem Restoration in Industry Clusters, Ministry of Education, Guangzhou 510006, PR China.

[c] Guangdong Provincial Key Laboratory of Solid Wastes Pollution Control and Recycling, Guangzhou 510006, PR China.

[d] Guangdong Engineering and Technology Research Center for Environmental Nanomaterials, Guangzhou 510006, PR China

[e] Guangdong Provincial Engineering and Technology Research Center for Environmental Risk Prevention and Emergency Disposal, Guangzhou, 510006, PR China.

[f] Department of Energy and Environment Engineering, Dawood University of Engineering and Technology, Karachi 74800, Pakistan.

[g] Department of Civil and Environmental Engineering, Hanyang University, Seoul, South Korea.

[*]Corresponding author: Pingxiao Wu

Tel: +86-20-39380538

Fax: +86-20-39383725

email: pppxwu@scut.edu.cn

1 Experimental section

1.1 Potentiometric titration experiment

The experimental procedure for potentiometric and conductometric titration was the same, as used in our previous study(Ahmed et al., 2020), in detail: A standard thermostatic bath was used to maintain temperature, inside which a specially designed glass bottle was placed; this bottle could accommodate measuring electrodes of conductivity and pH. A mechanical stirrer continuously stirred the suspensions for homogenization of the sample. A micropipette (ΔV=0.5% mL) was used to add the titrant volume, whereas pH and conductivity of the suspension were measured with a pH-meter a conductometer (Cond 730), respectively.

1.2 Determination of point of zero charge

The point of zero charge (pzc) of materials was calculated by the Roberts-Mular potentiometric titration method, which works on the ion exchange principle, by measuring sample pH at different ionic strength solutions(Mular and Roberts, 1966). A solution of 0.001 M NaCl was prepared using Milli-Q ultrapure water, and three sets of ten bottles were prepared, each containing 50 mL NaCl solution. Each set of ten bottles were adjusted in a range of 2~11 pH containing 1.00 g. of adsorbent (VER or HEX-VER). The ionic strength of each solution bottle was then raised to 0.01 and 0.1 mol.dm^{-3} by adding an appropriate amount of NaCl dry crystals. The bottles were shaken at 25 °C for 24 h, and after equilibrium, the final pH of the solutions was measured. The difference of pH (ΔpH) in initial pH (pH_i) and final pH (pH_f) was calculated by (Eq. (S1)) and was plotted against final pH. The pH value where ΔpH was zero indicated the point of zero charge (pzc) for each material.

$$\Delta\text{pH} = pH_i - pH_f \tag{S1}$$

1.3 Determination of surface charge density

Surface charge density was determined by acid-base potentiometric titration; the same procedure was used, as in our previous study(Ahmed et al., 2020), in detail: A blank solution (with a fixed concentration of electrolyte) or aqueous (VER or HEX-VER) suspension of 100 mL was poured in a glass bottle, which was thermostated at 25 ± 1 °C. A mixture of a fixed concentration of the blank solution of a given electrolyte and 0.5 ml of HCl (0.5 M) was mixed to 2 $g.L^{-1}$ of aqueous (VER or HEX-VER) suspension. The titrant solution (0.2 M NaOH) was added with 50 ± 0.005 µL increments; results were measured after pH and conductivity of the solution became constants. The titration was stopped around pH 10. Surface charge density σH was calculated as; the difference between the total amount of H^+ or OH^- added to the suspension by (Eq. (S4)) and that required to bring a blank solution with the same NaCl concentration at the same pH(Msadok et al., 2019; Schroth and Sposito, 1997).

$$pH = -log[H^+] \quad (S2)$$

$$[H^+] = 10^{-pH} \quad (S3)$$

$$\sigma H = \frac{V}{m} S \left\{ ([H^+]_b - [H^+]_s) - \left(\frac{k_w}{[H^+]_b} - \frac{k_w}{[H^+]_s} \right) \right\} \quad (S4)$$

where, σH is surface charge density ($mol.m^2$); V is the volume of the electrolyte solution (mL) equilibrated with the material(VER or HEX-VER); $[H^+]$ is the solution proton concentration; K_w is the dissociation product of water; subscripts "s" and "b" refer to sample and blank solution; m is the mass of sample (g), and S is the specific surface area ($m^2.g^{-1}$) calculated by Brunauer-Emmett-Teller (BET) analysis, as in (Table 1).

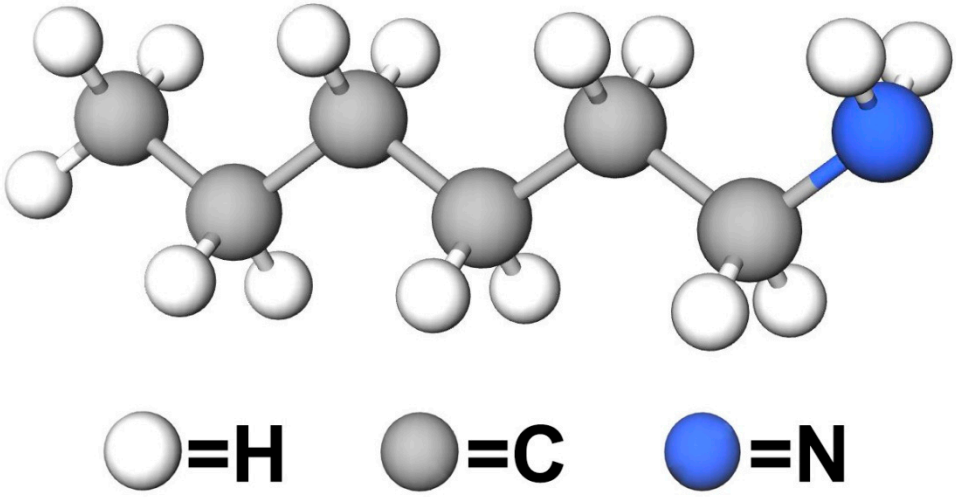

Figure S1. *The molecular structure of hexylamine [$CH_3(CH_2)_5NH_2$]*

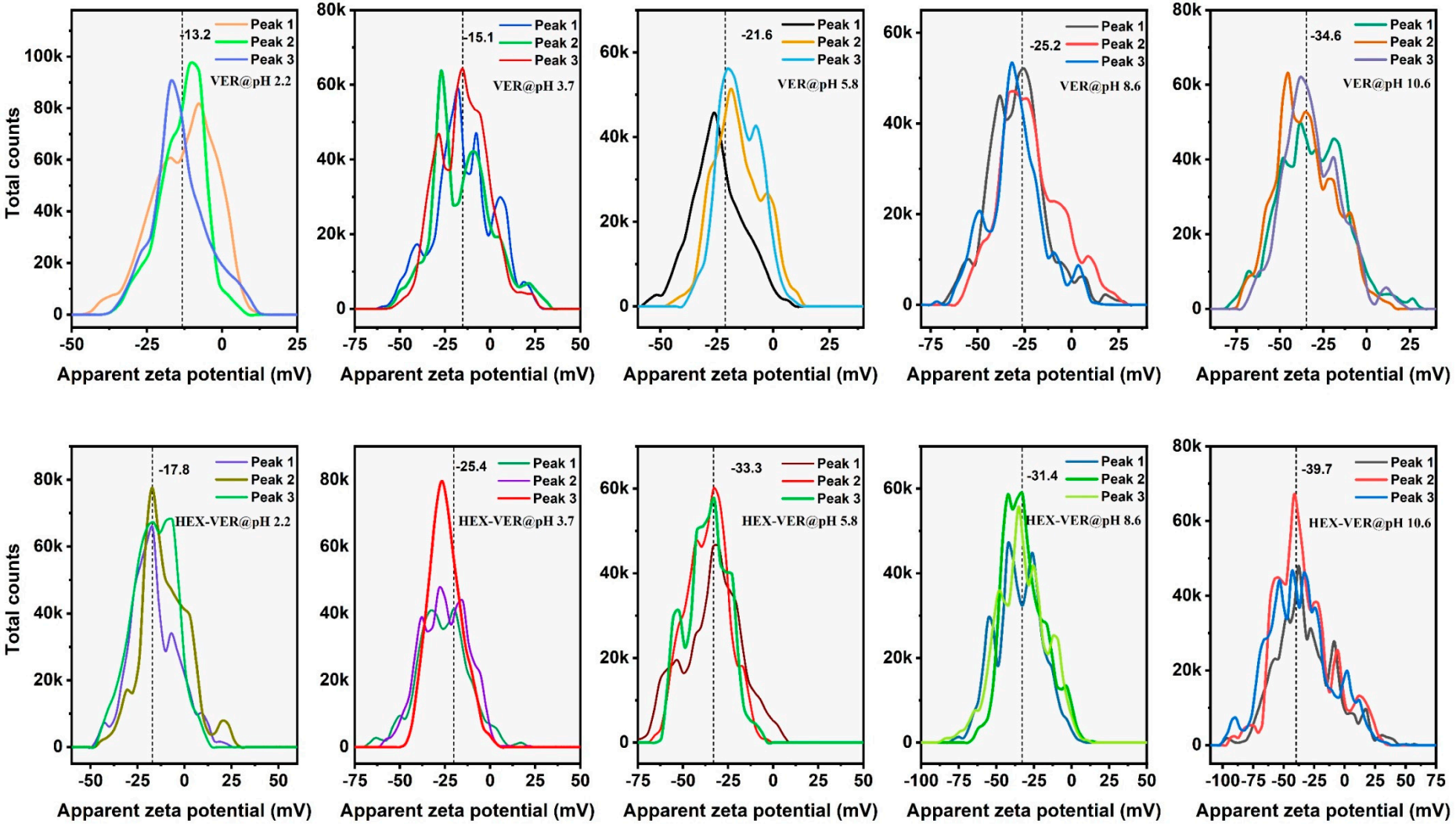

Figure S2*. Detailed zeta potential results of VER and HEX-VER in the pH range (2~11).*

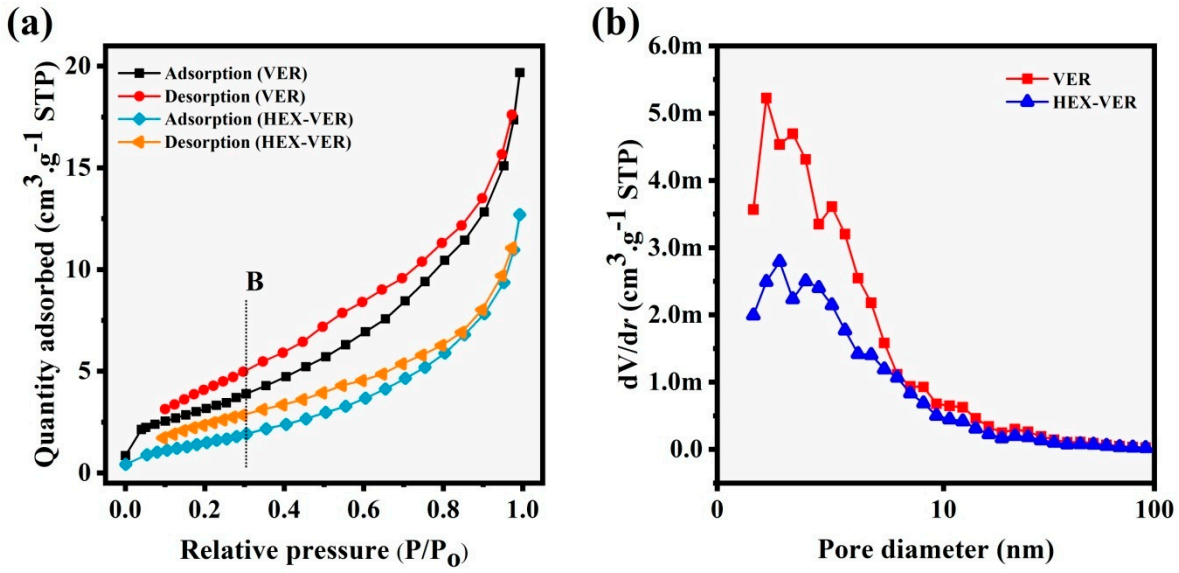

Figure S3. *Nitrogen adsorption-desorption curve (a) and pore diameter distribution (b) for VER and HEX-VER.*

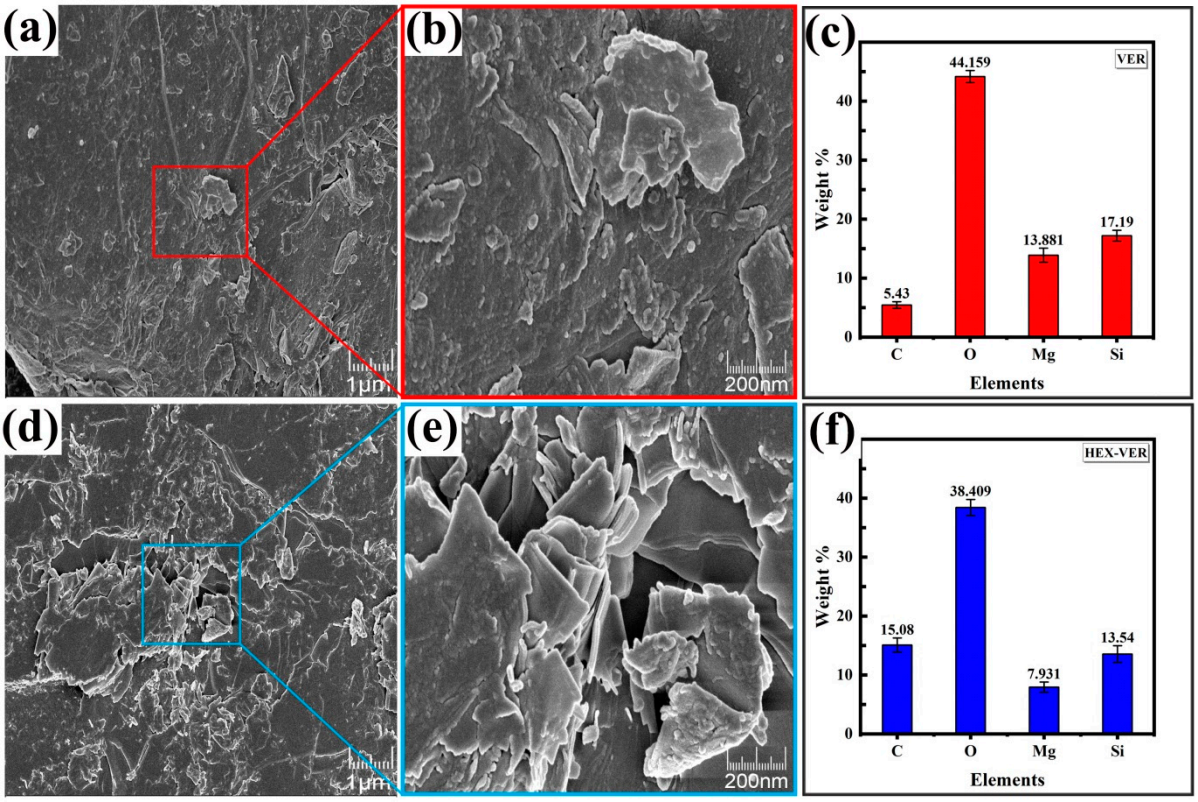

Figure S4. *Surface morphology (SEM images at 1 µm) of VER(a) and HEX-VER(d); zoomed SEM images (200 nm) of VER(b) and HEX-VER(e); and presence of major elements(Wt. %) in VER(c) and HEX-VER(f), respectively.*

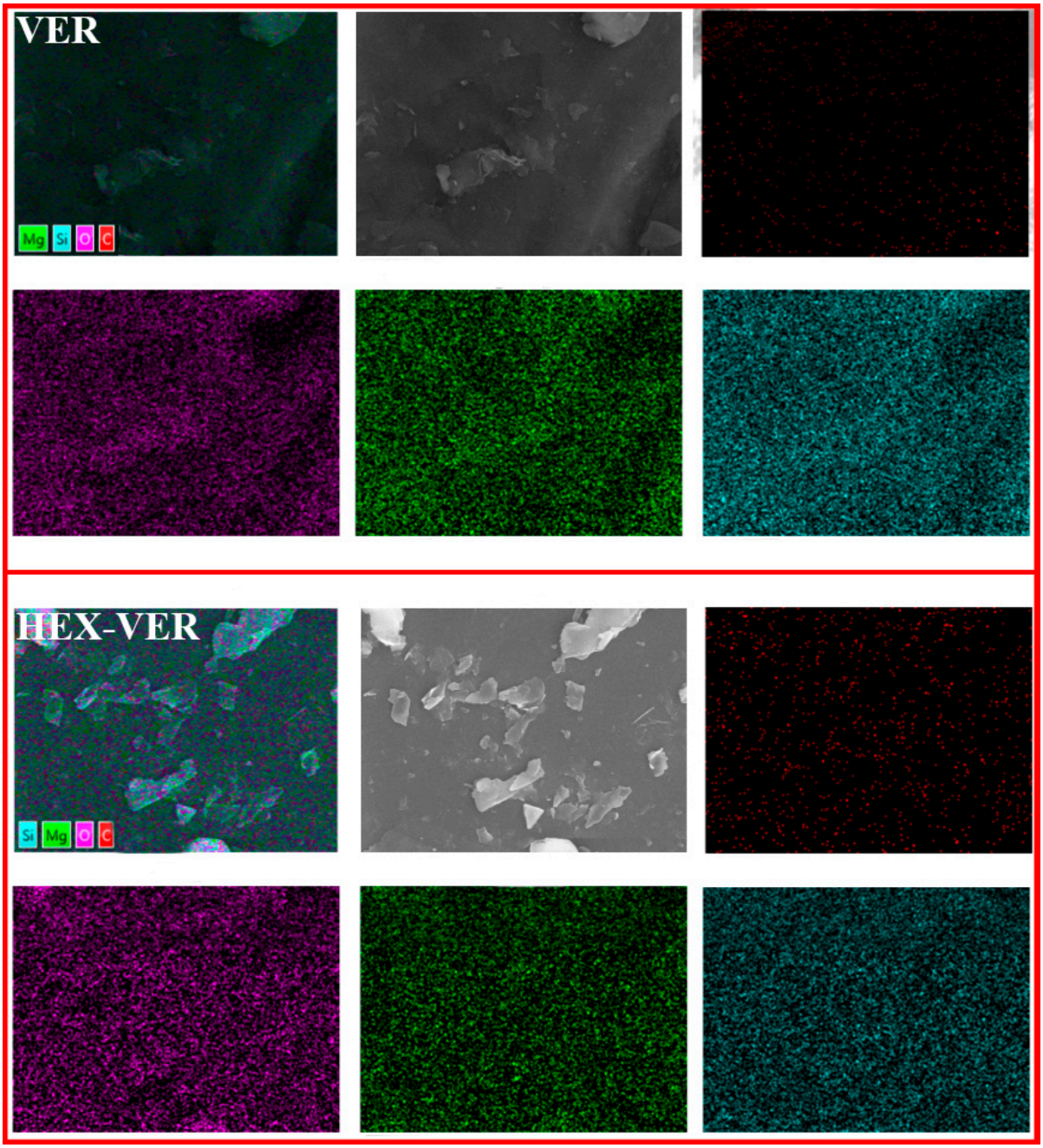

Figure S5 *Surface chemical composition of VER and HEX-VER by mapping.*

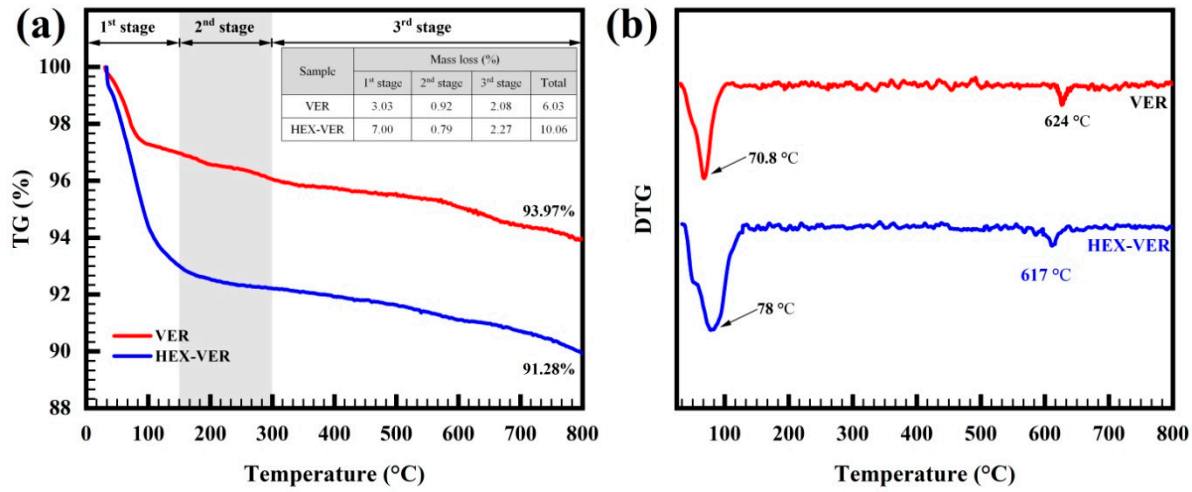

Figure S6. *TGA(a) and DTG(b) of VER and HEX-VER.*

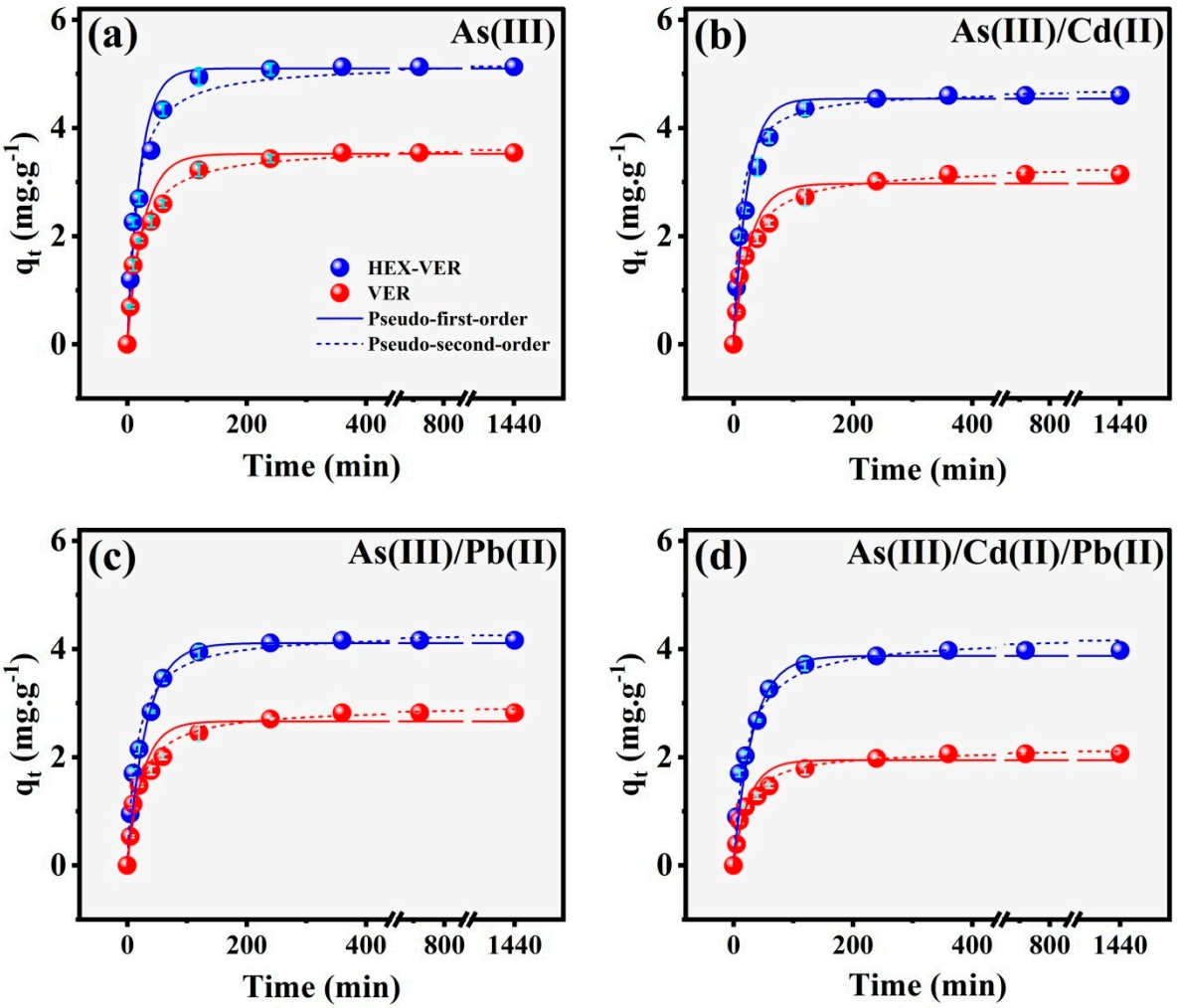

Figure S7. *Effect of contact time and kinetic study of As(III) singular (a), in the presence of Cd(II)(b), in the presence of Pb(II)(c), and in the presence of Cd(II)/Pb(II)(d) on VER and HEX-VER; (As(III) at C_i=30 mg.L^{-1}; contact time: 1440 min; temperature: 30 °C; pH: 5; adsorbent dosage: 1.0 g.L^{-1})*

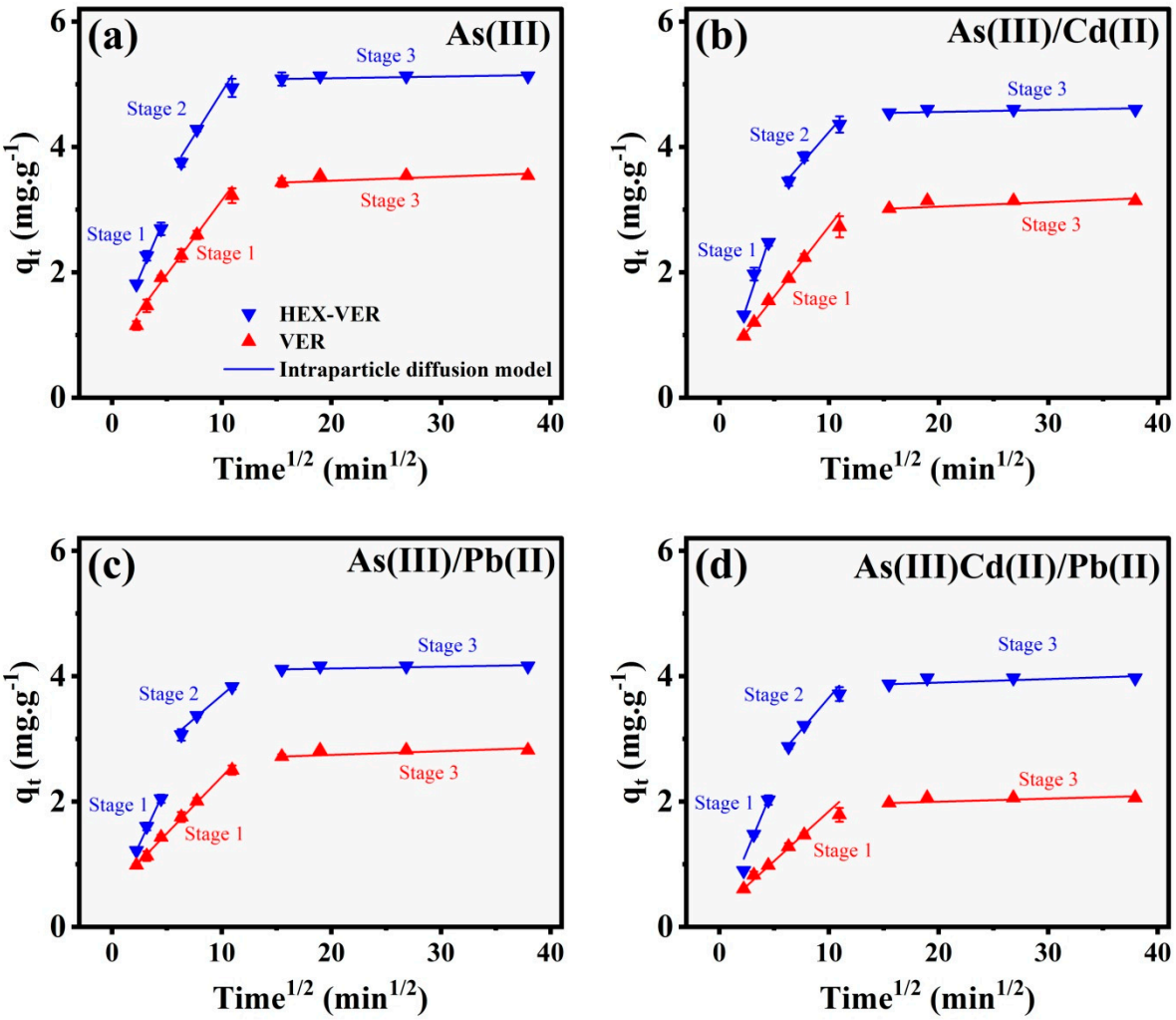

Figure S8. *Intraparticle diffusion model study of As(III) singular (a), in the presence of Cd(II)(b), in the presence of Pb(II)(c), and in the presence of Cd(II)/Pb(II)(d) on VER and HEX-VER; (As(III) at C_i=30 mg.L^{-1}; contact time: 1440 min; temperature: 30 °C; pH: 5; adsorbent dosage: 1.0 g.L^{-1})*

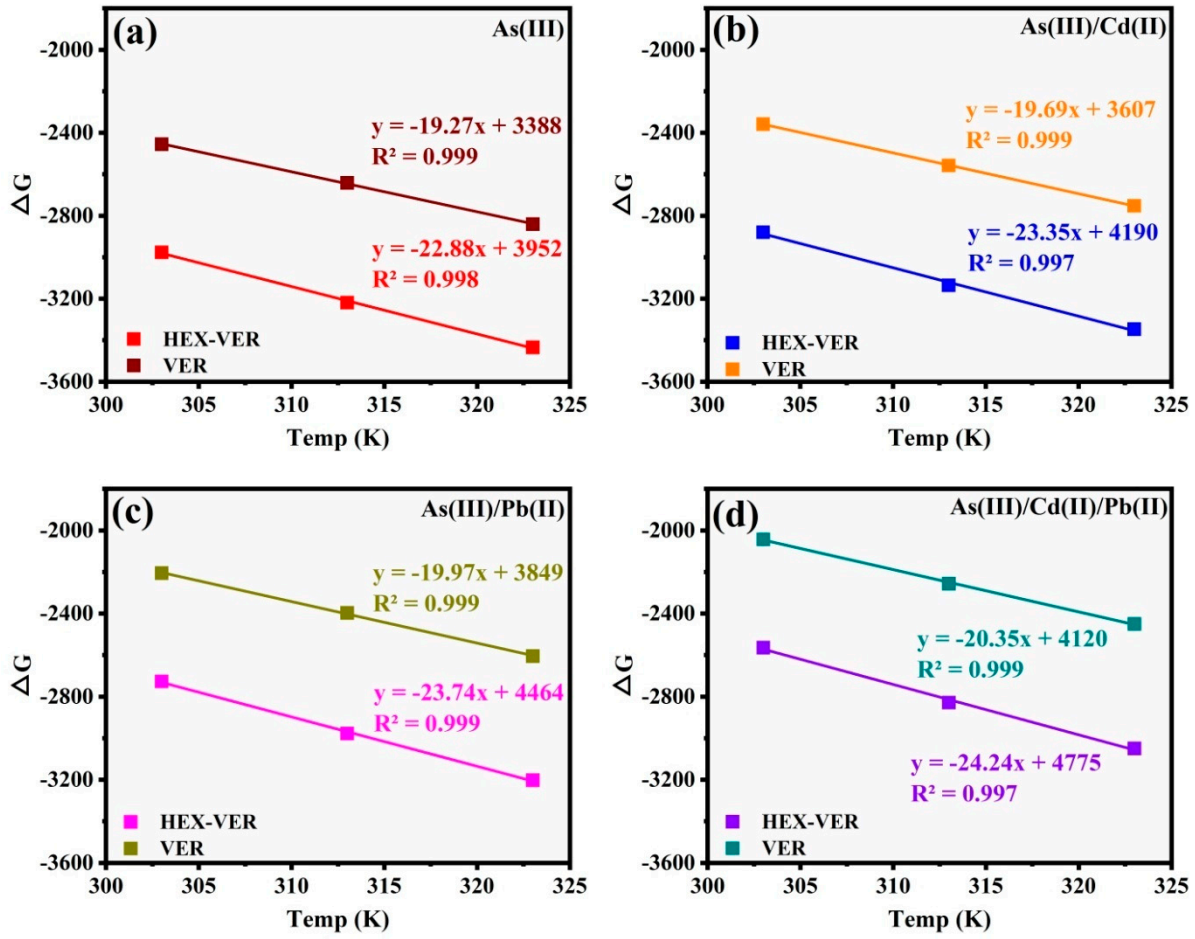

Figure S9. *Thermodynamic parameters for As(II) singular(a), and As(III) in the presence of Cd(II)(b), Pb(II)(c) and Cd(II)/Pb(II)(d) on VER and HEX-VER; (As(III) at C_i=30 mg.L^{-1}; contact time: 1440 min; temperature: 303 K to 323 K; pH: 5; adsorbent dosage: 1.0 g.L^{-1})*

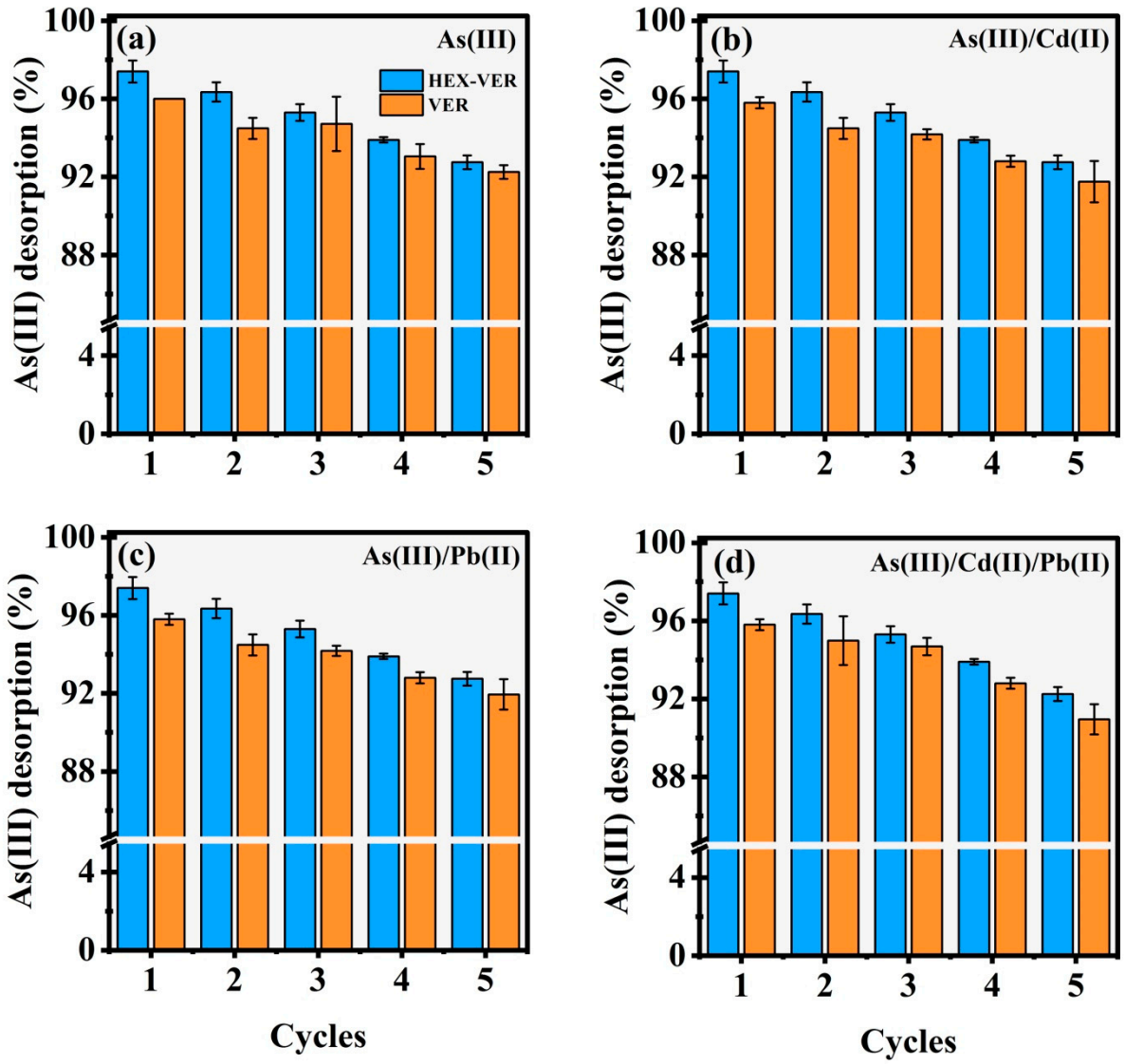

Figure S10. *Adsorption and desorption studies of As(III) singular (a); in the presence of Cd(II)(b); in the presence of Pb(II)(c) and in the presence of Cd(II)/Pb(II)(d), on VER and HEX-VER; adsorbent dosage: 1.0 g.L^{-1}; contact time: 1440 min; temperature: 30 °C; desorbent: 0.1 M NaOH; desorption time 240 min.*

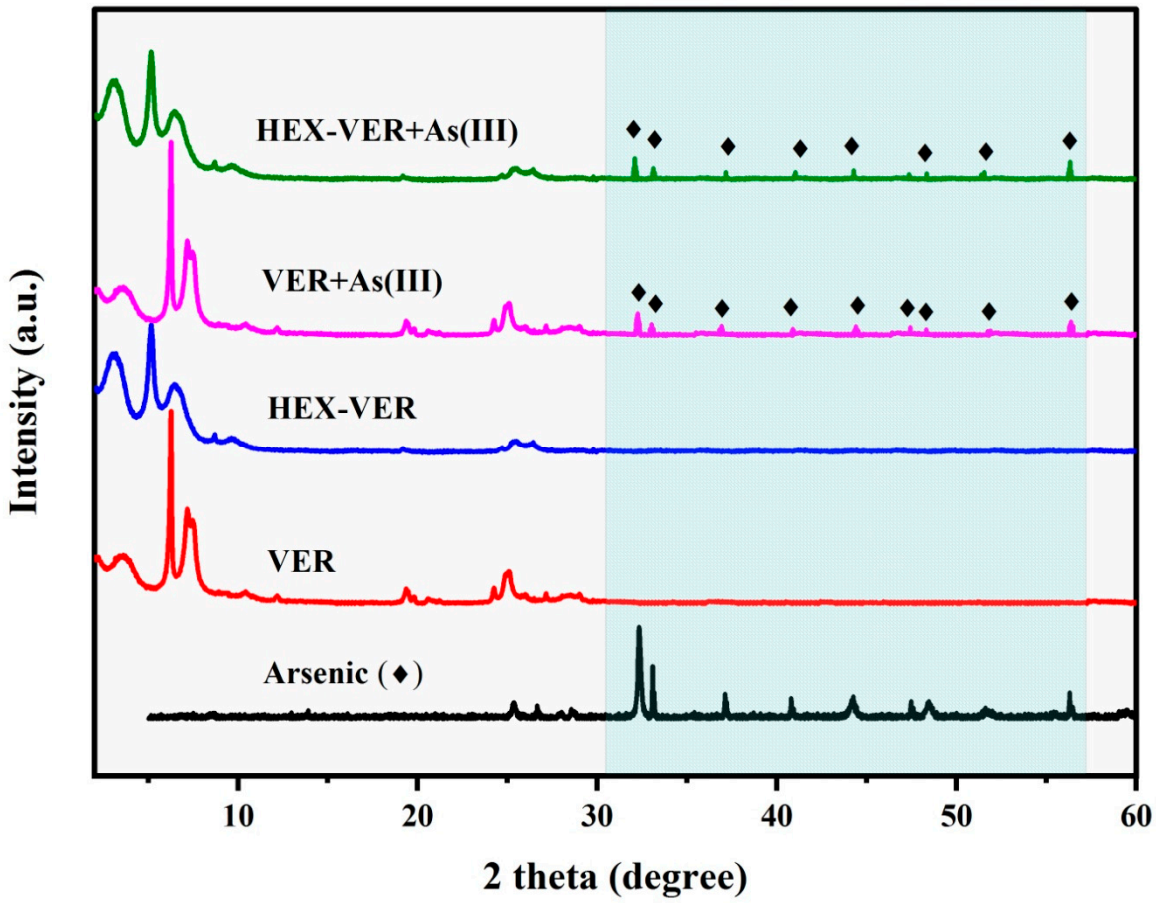

Figure S11. *XRD of VER and HEX-VER before and after the adsorption of As(III*).

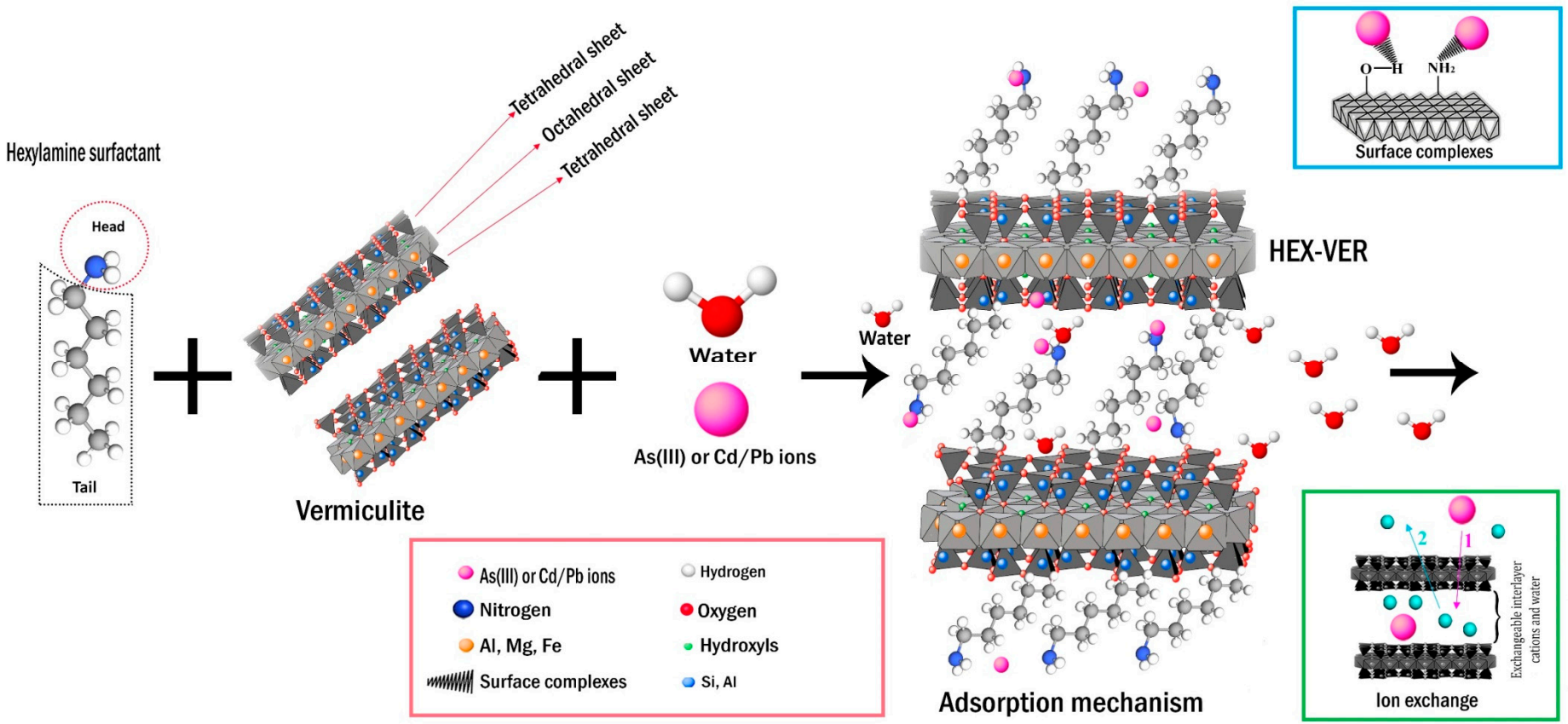

Figure S12. *Schematic diagram of removal mechanism of As(III) by hexylamine modified vermiculite.*

Table S1. *X-Ray Fluorescence Spectrometer (XRF) analysis of VER and HEX-VER*

Oxides	MASS (%)	
	VER	HEX-VER
SiO_2	37.76 ± 0.01	36.50 ± 0.01
MgO	20.76 ± 0.01	18.14 ± 0.01
Fe_2O_3	8.50 ± 0.01	8.66 ± 0.01
Al_2O_3	8.30 ± 0.01	8.26 ± 0.01
K_2O	4.38 ± 0.01	3.49 ± 0.01
CaO	3.97 ± 0.01	1.28 ± 0.01
P_2O_5	1.43 ± 0.01	0.89 ± 0.01
TiO_2	0.99 ± 0.01	1.10 ± 0.01
Cr_2O_3	0.10 ± 0.01	0.10 ± 0.01
MnO	0.07 ± 0.01	0.06 ± 0.01
NiO	0.07 ± 0.01	0.06 ± 0.01
L.O.I.	13.62 ± 0.01	21.46 ± 0.01

L.O.I.= Loss on ignition

Table S2. *Detailed information of all involved formulas of kinetics, isotherm and thermodynamic models.*

Type	Model	Equation	Parameters	
Formulas	Removal efficiency	$R\ (\%)\ = \frac{C_0 - C_t}{C_0} \times 100$	C_0 (mg·L^{-1}): initial As(III) concentration; C_t (mg·L^{-1}): residual As(III) concentration at *t* (min).	
	Adsorption capacity	$q_t = \frac{(C_0 - C_t)V}{m}$	*V (L):* reaction solution volume; *m (g):* the mass of the adsorbent.	
Isotherm model	Langmuir	$\frac{C_e}{q_e} = \frac{1}{q_m K_L} + \frac{C_e}{q_m}$ $R_{\mathrm{L}} = \frac{1}{1 + K_{\mathrm{L}} C_0}$	q_e(mg·g^{-1}): equilibrium adsorption capacity; C_e(mg·L^{-1}): solution equilibrium concentration; q_m(mg·g^{-1}): maximum adsorption capacity; K_L (L·mg^{-1}): Langmuir constant; R_L: the separation factor.	*(Langmuir, 1916)*
	Freundlich	$q_e = K_F c_e^{1/n}$ $\ln q_{\mathrm{e}} = \frac{1}{n} \ln C_{\mathrm{e}} + \ln K_{\mathrm{F}}$	K_F (L·mg^{-1}) and *n*: the Freundlich constants, which indicate the adsorption capacity and intensity.	*(Freundlich)*
Kinetics model	pseudo-first order	$\ln(q_e - q_t) = \ln q_e - k_1 t$	q_e (mg·g^{-1}): equilibrium adsorption capacity; q_t (mg·g^{-1}): the sorption amount at time t; k_1 (min^{-1}): the adsorption rate constant.	*(Corbett, 1972)*
	pseudo-second order	$\frac{t}{q_t} = \frac{t}{q_e} + \frac{1}{k_2 {q_e}^2}$	k_2 (g/mg min) : the rate constant determined by the plots of t/q_t versus *t*.	*(Ho and McKay, 1999)*
	intra-particle diffusion	$q_t = k_i t^{0.5} + c_i$	k_i (mg·g^{-1}·min$^{0.5}$): the rate constant; c_i: the intercept related to the thickness of the boundary layer.	*(Weber Jr and Morris, 1963)*
Thermodynamic model	Gibbs-Helmholtz equation	$\Delta G = -RT \ln K_d$ $\Delta G = \Delta H - T\Delta S$ $K_d = \frac{q_e}{c_e}$	*R*: the gas constant (8.314 J·mol^{-1}K^{-1}); *T* (K): the temperature; ΔG (kJ·mol^{-1}): the free energy change; ΔH (kJ·mol^{-1}): the enthalpy change; ΔS (kJ·Kmol^{-1}): the entropy change; K_d denotes distribution coefficient.	*(Atkins, 1978)*

Table S3. *The BET surface areas and pore parameters of the samples (S_{BET}, specific surface area by BET; D_a, average pore diameter; V_t, total porous volume)*

Parameters	Samples	
	VER	HEX-VER
S_{BET} ($m^2.g^{-1)}$	11.297	4.3225
D_a (nm)	10.576	16.684
BJH Meso $cm^3.g^{-1}$	0.0298	0.0180
V_t ($cm^3.g^{-1}$)	0.0306	0.0186

Table S4. *The surface chemical constituents of VER and HEX-VER*

Elements	VER Mass ratio (wt.%)			HEX-VER Mass ratio (wt.%)		
	Point 1	Point 2	Point 3	Point 1	Point 2	Point 3
C	5.03	5.18	6.15	14.23	14.28	16.74
O	43.38	45.56	43.43	39.38	37.13	38.81
Mg	13.34	13.16	15.17	8.64	7.18	7.98
Si	17.91	17.54	16.14	14.54	12.87	13.18
Al	6.07±1	5.84±1	5.74±1	5.34±1	5.45±1	5.88±1
K	6.72±1	6.26±1	6.65±1	6.71±1	5.87±1	5.38±1
Ca	0.77	0.68	0.64	0.74	0.59	0.63
Ti	0.45	0.39	0.43	0.39	0.37	0.41
Fe	6.32±1	5.37±1	5.64±1	5.61±1	4.45±1	4.21±1

***Table S5**. Isotherm parameters for As(III) adsorption on VER and HEX-VER.*

Pollutant	**Adsorbent**	**System**	**Langmuir parameters**			**Freundlich parameters**		
			q_{max} ($mg \cdot g^{-1}$)	K_L ($L \cdot mg^{-1}$)	R^2	$1/n_F$	K_F ($mg \cdot g^{1}$)($L \cdot mg^{-1}$)$^{1/n}$	R^2
As(III)	HEX-VER	As(III)	13.52	0.078	0.983	0.271	1.42	0.933
		As(III)/Cd(II)	12.12	0.080	0.977	0.285	1.22	0.963
		As(III)/Pb(II)	10.97	0.074	0.975	0.391	1.55	0.952
		As(III)/Cd(II)/Pb(II)	10.33	0.061	0.987	0.349	1.58	0.966
	VER	As(III)	11.89	0.084	0.989	0.299	0.83	0.982
		As(III)/Cd(II)	10.37	0.025	0.963	0.295	0.60	0.930
		As(III)/Pb(II)	9.32	0.062	0.961	0.243	0.76	0.931
		As(III)/Cd(II)/Pb(II)	6.12	0.018	0.979	0.257	0.43	0.966

***Table S6**. Kinetic parameters for As(III) adsorption on VER and HEX-VER.*

Pollutant	Adsorbent	System	q_e (experimental) (mg.g^{-1})	Pseudo first order model			Pseudo second order model		
				K_1 (min^{-1})	q_c (mg.g^{-1})	R^2	K_2 (g.mg^{-1}.min^{-1})	q_c (mg.g^{-1})	R^2
As(III)	HEX-VER	As(III)	5.13	5.12	0.045	0.923	0.014	5.13	0.933
		As(III)/Cd(II)	4.59	4.54	0.043	0.968	0.025	4.85	0.963
		As(III)/Pb(II)	4.16	4.10	0.031	0.966	0.010	4.47	0.988
		As(III)/Cd(II)/Pb(II)	3.97	3.87	0.031	0.987	0.010	4.21	0.988
	VER	As(III)	3.54	3.54	0.036	0.936	0.014	3.64	0.982
		As(III)/Cd(II)	3.13	4.85	0.012	0.991	0.013	3.27	0.994
		As(III)/Pb(II)	2.82	2.66	0.038	0.978	0.016	2.92	0.994
		As(III)/Cd(II)/Pb(II)	2.06	1.94	0.038	0.979	0.022	2.13	0.994

Table S7. *Parameters of Intra-particle diffusion model parameters for As(III) adsorption onto VER and HEX-VER.*

Pollutant	**Adsorbent**	**System**	**Stage 1** Surface diffusion			**Stage 2** Intraparticle diffusion			**Stage 3** Ultimate adsorption equilibrium		
			K_1	C_1	R^2	K_2	C_2	R^2	K_3	C_3	R^2
As(III)	HEX-VER	As(III)	0.889	0.4133	0.995	2.099	0.2773	0.965	5.041	0.0027	0.843
		As(III)/Cd(II)	0.150	0.5239	0.996	2.227	0.2011	0.980	4.492	0.0032	0.846
		As(III)/Pb(II)	0.377	0.3767	0.998	2.204	0.1491	0.994	4.063	0.0029	0.988
		As(III)/Cd(II)/Pb(II)	0.148	0.4196	0.999	1.618	0.2038	0.984	3.783	0.0057	0.847
	VER	As(III)	0.786	0.2356	0.984	-	-	-	3.335	0.0062	0.982
		As(III)/Cd(II)	0.491	0.2239	0.998	-	-	-	2.901	0.0072	0.847
		As(III)/Pb(II)	0.589	0.1804	0.998	-	-	-	2.626	0.0058	0.846
		As(III)/Cd(II)/Pb(II)	0.254	0.1590	0.997	-	-	-	1.901	0.0048	0.994

Table S8: *Thermodynamic parameters for single and simultaneous As(III) adsorption on VER and HEX-VER.*

Pollutant	Adsorbent	System	T(K)	△G kJ mol^{-1}	△H kJ mol^{-1}	△S J mol^{-1}K^{-1}
As(III)	VER	As(III)	303	-1.68003	7.887	0.03157434
			313	-1.95458		
			323	-2.31068		
		As(III)/Cd(II)	303	-1.47372	7.448	0.02944461
			313	-1.77776		
			323	-2.06282		
		As(III)/Pb(II)	303	-5.12649	16.582	0.07164519
			313	-5.73111		
			323	-6.55699		
		As(III)/Cd(II)/Pb(II)	303	-4.94107	15.432	0.06723784
			313	-5.58658		
			323	-6.28521		
	HEX-VER	As(III)	303	-5.47350	13.604	0.06296204
			313	-6.16903		
			323	-6.73415		
		As(III)/Cd(II)	303	-5.31851	11.886	0.05678055
			313	-5.80497		
			323	-6.45238		
		As(III)/Pb(II)	303	-9.06573	23.741	0.108273
			313	-10.33750		
			323	-11.23530		
		As(III)/Cd(II)/Pb(II)	303	-8.95409	21.278	0.09977587
			313	-9.99450		
			323	-10.95050		

Table S9. *Comparison of maximum adsorption capacities (Q_{max}) of As(III) by different materials*

Adsorbent	Initial pH	Q_{max} As(III) ($mg \cdot g^{-1}$)	References
Fe-Mn binary oxide	pH 7.0	114	(Zhang et al., 2012)
Zn-Fe mixed metal oxides	pH 7.0	36	(Di et al., 2017)
Cu doped Fe_3O_4	pH 5.0	38.0	(Wang et al., 2015)
CMZF	pH 6.0	90.197	(Liu et al., 2019)
3-aminopyrazole functionalized graphene oxide	pH 8.3	131.57	(Alimohammady et al., 2017)
Zeolite-supported zero-valent iron	pH 6.0	18.73	(Li et al., 2018)
Calcium based magnetic biochar	pH 5.2	6.34	(Wu et al., 2020)
Iron/calcium impregnated carbon (GL200)	pH 7.0	3.385	(Gong et al., 2020)
HEX-VER	pH 5.0	**13.52**	**This work**

***Table S10**. Water quality index of Pearl River (ZhuJiang, Guangdong, China) water samples used in this study*

Adsorbent	Water-quality Index	Values
Anions	NO_3^- ($mg.L^{-1}$)	3.41
	SO_4^{2-} ($mg.L^{-1}$)	9.67
	PO_4^{3-} ($mg.L^{-1}$)	0.28
Cations	Ca^{2+} ($mg.L^{-1}$)	17.64
	Mg^{2+} ($mg.L^{-1}$)	7.1
	Zn^{2+} ($mg.L^{-1}$)	0.54
Spiked metals	As(III) ($\mu g.L^{-1}$)	2000
	Cd(II) ($\mu g.L^{-1}$)	4000
	Pb(II) ($\mu g.L^{-1}$)	4000
Other	pH	7.26
	TOC ($mg.L^{-1}$)	5.64

References

Ahmed, Z, Wu, P, Jiang, L, Liu, J, Ye, Q, Yang, Q, Zhu, N, 2020. Enhanced simultaneous adsorption of Cd(II) and Pb(II) on octylamine functionalized vermiculite. Colloids and Surfaces A: Physicochemical and Engineering Aspects 604:125285.

Alimohammady, M, Jahangiri, M, Kiani, F, Tahermansouri, H, 2017. Highly efficient simultaneous adsorption of Cd(ii), Hg(ii) and As(iii) ions from aqueous solutions by modification of graphene oxide with 3-aminopyrazole: central composite design optimization. New Journal of Chemistry 41:8905-8919.

Atkins, P W, 1978. Physical chemistry. Oxford University Press: Oxford.

Corbett, J F J J o C E, 1972. Pseudo first-order kinetics. 49:663.

Di, G, Zhu, Z, Zhang, H, Zhu, J, Lu, H, Zhang, W, Qiu, Y, Zhu, L, Küppers, S, 2017. Simultaneous removal of several pharmaceuticals and arsenic on Zn-Fe mixed metal oxides: Combination of photocatalysis and adsorption. Chemical Engineering Journal 328:141-151.

Freundlich, H J J o P, F. 1906. Over the adsorption in solution. 57:385.

Gong, X-J, Li, Y-S, Dong, Y-Q, Li, W-G, 2020. Arsenic adsorption by innovative iron/calcium in-situ-impregnated mesoporous activated carbons from low-temperature water and effects of the presence of humic acids. Chemosphere 250:126275.

Ho, Y-S, McKay, G J P b, 1999. Pseudo-second order model for sorption processes. 34:451-465.

Langmuir, I, 1916. THE CONSTITUTION AND FUNDAMENTAL PROPERTIES OF SOLIDS AND LIQUIDS. PART I. SOLIDS. Journal of the American Chemical Society 38:2221-2295.

Li, Z, Wang, L, Meng, J, Liu, X, Xu, J, Wang, F, Brookes, P, 2018. Zeolite-supported nanoscale zero-valent iron: New findings on simultaneous adsorption of Cd(II), Pb(II), and As(III) in aqueous solution and soil. Journal of Hazardous Materials 344:1-11.

Liu, J, Wu, P, Li, S, Chen, M, Cai, W, Zou, D, Zhu, N, Dang, Z, 2019. Synergistic deep removal of As(III) and Cd(II) by a calcined multifunctional MgZnFe-CO3 layered double hydroxide: Photooxidation, precipitation and adsorption. Chemosphere 225:115-125.

Msadok, I, Hamdi, N, Gammoudi, S, Rodríguez, M A, Srasra, E, 2019. Effect of cationic surfactant HDPy+ on the acidity and hydrophilicity of Tunisian clay. Materials Chemistry and Physics 225:279-283.

Mular, A, Roberts, R, 1966. A simplified method to determine isoelectric points of oxides. Canadian Mining and Metallurgical Bulletin 59:1329-&.

Schroth, B K, Sposito, G, 1997. Surface charge properties of kaolinite. Clays and Clay Minerals 45:85-91.

Wang, T, Yang, W, Song, T, Li, C, Zhang, L, Wang, H, Chai, L, 2015. Cu doped Fe3O4 magnetic adsorbent for arsenic: synthesis, property, and sorption application. RSC Advances 5:50011-50018.

Weber Jr, W J, Morris, J C J J o t s e d, 1963. Kinetics of adsorption on carbon from solution. 89:31-59.

Wu, J, Li, Z, Huang, D, Liu, X, Tang, C, Parikh, S J, Xu, J, 2020. A novel calcium-based magnetic biochar is effective in stabilization of arsenic and cadmium co-contamination in aerobic soils. Journal of Hazardous Materials 387:122010.

Zhang, G, Liu, H, Qu, J, Jefferson, W, 2012. Arsenate uptake and arsenite simultaneous sorption and oxidation by Fe–Mn binary oxides: Influence of Mn/Fe ratio, pH, Ca2+, and humic acid. Journal of Colloid and Interface Science 366:141-146.